Journal of Catalysis **198,** 338–347 (2001)
doi:10.1006/jcat.2000.3140, available online at http://www.idealibrary.com on IDEAL®

# Oxidative Methanol Reforming Reactions on CuZnAl Catalysts Derived from Hydrotalcite-like Precursors

S. Murcia-Mascarós,* R. M. Navarro,* L. Gómez-Sainero,* U. Costantino,† M. Nocchetti,† and J. L. G. Fierro*,[1]

*Institute of Catalysis and Petrochemistry, CSIC, Cantoblanco, 28049 Madrid, Spain; and †Department of Chemistry, University of Perugia, Via Elce di Sotto 8, 06123 Perugia, Italy

Received September 28, 2000; revised November 24, 2000; accepted November 24, 2000; published online February 13, 2001

**Copper–zinc–aluminum (CZA) catalysts prepared by the homogeneous precipitation of chloride salts in the presence of urea to produce hydrogen selectively by partial oxidation and oxyreforming reactions of methanol were used. The crystalline phases of the precursors and of the air-calcined CZA samples were identified by X-ray diffraction. Temperature-programmed reduction revealed that both CuO and $CuAl_2O_4$ phases were present in the calcined catalysts. Prereduced catalysts were tested in both partial oxidation ($O_2/CH_3OH = 0.3$–$0.4$) and oxyreforming reactions ($O_2/CH_3OH/H_2O = 0.3 : 1 : 1.1$) of methanol exhibiting high activity for $CH_3OH$ conversion and very high selectivity for $H_2$ production. The product distributions obtained in the partial oxidation of methanol (POM) reaction as a function of $CH_3OH$ and $O_2$ conversion indicate clearly that both conversion and selectivity become strongly dependent on the $O_2$ concentration in the gas phase and much less on the catalyst composition investigated. At low methanol conversion, when $O_2$ is not completely consumed, combustion and decomposition of methanol are the dominant reactions, however when $O_2$ is near or completely consumed, the methanol conversion goes beyond the expected stoichiometric POM values (60 and 80% for $O_2/CH_3OH$ molar ratios of 0.3 and 0.4, respectively). For the oxyreforming reaction, the simultaneous increase in $H_2$ selectivity at the expense of water, with a less marked increase of CO selectivity, points to the contribution of steam reforming of methanol. The Auger parameter of copper of the catalysts used in the partial oxidation (1849.1 eV) and in the oxyreforming (1849.3 eV) reactions indicates that $Cu_2O$ species are present on the active catalyst surface. These $Cu_2O$ structures, developed on the catalyst surface during on-stream operation, appear to be sufficiently large to be also observed by X-ray diffraction of the catalysts used in both reactions.**



## INTRODUCTION

There is growing incentive to develop clean electric power sources for vehicles and stationary power plants. This interest stems not only from the need for an alternative energy source for the decreasing supply of fossil fuels but also from the increasingly stringent environmental regulations coming into effect in many countries. A promising technology, which is actively being developed, is the proton-exchanged membrane (PEM) fuel cell, which uses the chemical energy stored in the H–H bond to produce electricity. Because of safety, onboard $H_2$ generation by reforming of a liquid fuel is being extensively studied for commercialization. Among the liquid fuel to be reformated, methanol remains prominent because of its low cost, ease of handling, and high energy density (1). Hydrogen can be obtained directly from methanol according to three different processes: thermal decomposition, partial oxidation (POM), and steam reforming (SRM). Under specific reaction conditions, POM and SRM produce almost quantitatively $H_2$ and $CO_2$:

$$CH_3OH + \frac{1}{2}O_2 \rightarrow 2H_2 + CO_2 (\Delta H^\circ = -192.2 \text{ kJ/mol}) \quad [1]$$

$$CH_3OH + H_2O \rightarrow 3H_2 + CO_2 (\Delta H^\circ = +49.4 \text{ kJ/mol}). \quad [2]$$

While POM is exothermic, SRM is endothermic, and produces a more favorable $H_2/CO_2$ ratio. Another option is to combine reactions [1] and [2] by cofeeding simultaneously oxygen steam and methanol through the oxidative methanol reforming (OMR). In this process, the ratio of the three reactants can be chosen such that the overall reaction heat is nearly neutral, which means that the heat necessary to maintain SRM is supplied by the POM reaction. In addition to these reforming reactions, the reverse shift reaction takes place simultaneously. Thus, the product gas also contains CO:

$$CO_2 + H_2 \rightarrow H_2O + CO (\Delta H^\circ = +41.0 \text{ kJ/mol}). \quad [3]$$

In our previous work (2), we examined the POM reaction over $Cu/ZnO(Al_2O_3)$ catalysts in the absence of steam and found that $CO_2$ selectivity was substantially higher than

[1] To whom correspondence should be addressed. Fax: +34 91 585 4760. E-mail: jlgfierro@icp.csic.es.



0021-9517/01 $35.00

that observed for SRM and that the rate of POM was a strong function of the copper content. Similarly, ZnO- (3, 4) and $ZrO_2$-supported Pd catalysts (5) were also found to be highly active and selective for POM to $H_2$, $CO_2$, and CO. While SRM for hydrogen production has been extensively investigated (6–8), there have been fewer reports for OMR (9, 10). Huang and co-workers (9, 10) studied the effect of addition of oxygen to the SRM reaction, and determined the kinetics of the OMR overreduced CuZnAl catalysts. These authors proposed that the rate of the combined OMR process could be calculated by the sum of the rates of POM and SRM reactions. In line with this, it appeared of interest to compare in this article the performance of CuZnAl catalysts under the conditions of POM and OMR reactions, because beneficial effects in terms of $H_2$ productivity under nearly neutral heat balance shoud be expected for the OMR reaction (11). According to our previous experience in the POM reaction (2, 3, 5), and considering that hydrotalcite-like compounds yield a great variety of mixed oxides upon calcination (see, e.g., Ref. (11) and references therein), the CuZnAl catalysts selected for the comparison of POM and OMR reactions were prepared from thermal decomposition of the hydrotalcite-like (HTlc) precursors.

It is known (12) that hydrotalcite-like compounds, also called layered double hydroxides, are an important class of lamellar solids represented by the general formula $[M(\mathrm{II})_{1-x}M(\mathrm{III})_x(\mathrm{OH})_2]^{x+}\,[A^{z-}_{x/z}\cdot m\mathrm{H_2O}]^{x-}$, where $M(\mathrm{II}) =$ Mg, Zn, Ni, Cu, etc., $M(\mathrm{III}) =$ Al, Fe, Cr, etc., and $A^{z-} = CO_3^{2-}$ $SO_4^{2-}$, $Cl^-$, etc. The lamellae, of brucite type, are built up by concatenation through the edges of octahedra, the centers of which are occupied by metal cations and the vertices by hydroxide ions. The interlayer regions contain exchangeable anions. HTlc are extensively studied and applied as catalysts, precursors, and supports of catalysts due to the wide range of preparation variables that allows the formation of precipitates having a homogeneous cation distribution. Moreover, thermal decomposition of these HTlc leads to the formation of homogeneous and stable mixtures of oxides having catalytic properties. It is also known that the insertion of copper ions into the brucite-like sheet is unfavored because of the Jahn–Teller effect, showed by these ions, which produces a distorted octahedral disposition of OH groups around the copper ion. It has been however found (12) that the presence of other divalent cations, such as Mg(II), Zn(II), and Co(II), favors the accommodation of Cu(II) into the sheet, giving rise to ternary hydrotalcite phases.

It was thus conceivable to attempt the preparation of CuZnAl catalysts from HTlc precursors. The procedure selected in this paper to prepare these HTlc precursors basically included slow coprecipitation from "homogeneous solution" of Cu(II), Zn(II), and Al(III) cations, which usually leads to precipitates mainly comprising ternary CuZnAl–HTlc. Then the CuZnAl systems were tested in both POM and OMR reactions, and the effect of several reaction parameters, e.g., temperature, $O_2/CH_3OH$ ratio, and presence of steam, on the performance was studied. Excellent performance in terms of $H_2$ selectivity and very low levels of CO, a key requirement for PEM fuel cell applications, were found in the OMR process over CuZnAl catalysts derived from hydrotalcite-like precursors.

## EXPERIMENTAL PROCEDURE

### *Catalyst Preparation*

Aqueuos solutions of copper(II), zinc, and aluminum, 0.5 mol/L, were used to obtain CuZnAl–hydrotalcite-like precursors following a relatively new procedure (13) based on the *in situ* formation of ammonium carbonate accomplished by the hydrolysis of urea at 363–373 K.

The sample, hereafter indicated CZA1, has been obtained from the above solutions in the Cu(II)/Zn(II) and Zn(II)/Al(III) molar ratios of 2.5 and 3.0, respectively. For the sample indicated CZA2, the Cu(II)/Zn(II) and Zn(II)/Al(III) molar ratios were 2.0 and 1.0, respectively. For the sample indicated CZA3, the Cu(II)/Zn(II) and Zn(II)/Al(III) molar ratios were 0.4 and 1.3, respectively. The original synthetic procedure was slightly modified as follows: solid urea (Panreac, reagent grade) was dissolved at room temperature into a solution containing $ZnCl_2$ and $AlCl_3$ (Panreac) in the selected molar ratio until a molar ratio urea/Al(III) equal to 10 was reached. When this solution becomes opalescent at 363 K, a selected volume of 0.5 M $CuCl_2$ (Panreac) solution was dropwise added to the slurry while mantained at 363 K under vigorous stirring. The resulting precipitate was left to digest at this temperature for further 24 h under stirring. The solids were filtered out, washed until pH 6, dried at 353 K for 16 h, and finally calcinated at 723 K.

### *Catalyst Characterization*

The catalyst precursors, as well as the fresh and used catalyst, were characterized by X-ray diffractometry according to the step-scanning procedure (step size 0.02°) using a computerized Seifert 3000XRD diffractometer using Cu$K\alpha$ radiation, a PW 2200 goniometer Bragg-Brentano $\theta/2\theta$, provided with a bent graphite monochromator and an automatic slit.

Chemical composition of the catalysts was determined by inductively coupled plasma atomic emission spectroscopy (ICP-AES), Perkin–Elmer Optima 3300DV inductively coupled plasma emission spectroscopy. The solid catalyst was first treated with acqua regia at 363 K, then an aqueous solution of HF was added while maintaining the same temperature.

The specific areas were calculated by the BET method from the $N_2$ (Air Liquide, 99.994%) adsorption isotherms

recorded in an ASAP 2010 equipment at 77 K and taking a value of 0.1620 $nm^2$ for the cross section of the physically adsorbed $N_2$ molecule. Thermogravimetric curves were obtained with a Perkin–Elmer TGS-2 equipment coupled with Data Station 3700 and temperature controller system 7/4. A heating rate of 5 K/min and an air flow rate of 30 mL/min were used. Temperature-programmed reduction (TPR) experiments were carried out in a semiautomatic Micromeritics TPD/TPR 2900 apparatus fitted with a TC detector and interfaced to a microcomputer. Samples of 0.050 g were pretreated in a He (Air Liquide, 99.996%) stream at 673 K for 0.5 h and then the TPR experiment was run in a stream of 10% $H_2$/Ar (Air Liquide) flow (50 mL/min), heating the sample at a rate of 10 K/min up to 800 K.

X-ray photoelectron spectra (XPS) were acquired with a VG Escalab 200R spectrometer using Mg$K\alpha$ X-ray source ($h\upsilon = 1253.6$ eV, 1 eV $= 1.602 \times 10^{-19}$ J). Calcined and used catalysts were analyzed. The catalysts used were quenched to room temperature and immediately drenched in i-octane under nitrogen to avoid oxidation of copper by exposure to air. The C 1*s*, Zn 2*p*, Al 2*p*, and Cu 2*p* core-level spectra were recorded and the corresponding binding energies (BE) referenced to the C 1*s* line at 284.9 eV (accuracy within $\pm 0.1$ eV). The $Cu_{LMM}$ Auger peak was also recorded and the modified Auger parameter ($\alpha_A$) calculated by the equation $\alpha_A = h\upsilon +$(KE $Cu_{LMM}$-KE Cu $2p_{3/2}$), where the difference in parentheses represents the difference in kinetic energy of the Auger electron and the Cu $2p_{3/2}$ photoelectron.

### *Catalytic Activity*

Partial oxidation of methanol was studied either in absence (POM) or in the presence of water (OMR) using a fixed-bed flow reactor in the temperature range 473–633 K at atmospheric pressure. Activity tests were performed using 0.2 g of catalyst diluted with SiC (both in the 0.4–0.5 mm particle size) at a volume ratio of 2 : 1 to avoid adverse thermal effects (11). The catalyst bed was placed in a 6-mm I.D. stainless steel tubular reactor with a coaxially centered thermocouple. Prior to the reaction and between different runs, the catalysts were flushed in nitrogen at 423 K followed by reduction *in situ* at 723 K (heating rate 5 K/min) with 40 mL/min of 10 vol% $H_2/N_2$ mixture for 2 h. The pretreating gases were flushed from the reactor with $N_2$ before admission of methanol–oxygen–water–nitrogen reaction mixtures. Methanol and water were fed independently into the preheater by means of a liquid pump (Becton-Dickinson) before mixing with oxygen and nitrogen (balance) streams. The gas flows were adjusted with Brooks model 5850E mass flow controllers. For the POM reaction, the reactants were introduced into the reactor in the molar ratio $O_2/CH_3OH = 0.3$–$0.4$, whereas for OMR a ratio $O_2/CH_3OH/H_2O = 0.3/1/1.1$ was used. In both tests, the total flow rate was kept at 120 mL/min (STP) (GHSV $=$ 32,700 $h^{-1}$) and the methanol concentration in the feed gas mixture was fixed at 21.4 vol%. These conditions were selected in order to avoid thermal effects derived from the high exothermicity of the reaction.

The reaction products were analyzed on-line by GC with TCD (Varian chromatograph Model Star 3400 CX) equipped with Porapack Q ($CO_2$, water, methanol, formaldehyde, methyl formate, and dimethyl ether) and molecular sieve 5A ($H_2$, $O_2$, $N_2$, CO) packed columns connected in series, using He as carrier gas. Activity was measured at reaction temperatures between 473 and 633 K running from the lowest to the highest temperature and mantaining the reaction 4 h at each temperature. Steady-state values of methanol conversion (reached when the difference in methanol conversion bewteen subsequent analyses is lower than $\pm 2\%$) are the average of two different analyses taken after 3 h of on-stream operation at a given temperature.

## RESULTS AND DISCUSSION

### *Catalyst Characterization*

Table 1 shows the chemical composition, expressed as atomic percentage, and textural parameters of the calcined catalysts. The BET area of the CZA-3 catalyst, containing a higher proportion of aluminum, is substantially higher than that for its CZA-1 and CZA-2 counterparts, with lower Al-loading. As can be seen below (Fig. 3), a part of the aluminum forms surface copper–aluminate phases.

Thermogravimetric analysis (TGA) of the representative CZA-2 precursor revealed that the sample undergoes decomposition through consecutive steps (Fig. 1). Three major decomposition steps can be identified: (i), the first, ranging from 298 to 400 K, is associated with water removal; (ii) the second in the temperature region from 400 to 625 K is assigned to the dehydroxylation and decarbonation reactions (13). Although both processes are clearly separated in the derivative curve (dashed line in Fig. 1), some overlap among them is visible in the integral TGA curve. (iii) The last ranging from 625 to 850 K is ascribed to hydrochloric acid removal. The broad peak observed in the derivative curve for step (iii) most likely involves contributions of several crystalline chlorine-containing phases identified by X-ray diffraction (see below in Fig. 2).

**TABLE 1**

**Composition (Atom Ratio %), Specific Area, and Maximum Temperature for $H_2$ Reduction of CZA Catalysts**

| | Composition (%) | | | $S_{BET}$ | TPR (K) | | *d* (nm) | |
|---|---|---|---|---|---|---|---|---|
| Catalyst | Cu | Zn | Al | ($m^2$/g) | Onset | Max | CuO | ZnO |
| CZA-1 | 72.4 | 16.4 | 10.8 | 23 | 460 | 588 | 26 | 40 |
| CZA-2 | 54.3 | 18.7 | 26.6 | 73 | 435 | 653 | 34 | 46 |
| CZA-3 | 21.9 | 37.1 | 40.9 | 143 | 420 | 720 | 33 | 81 |

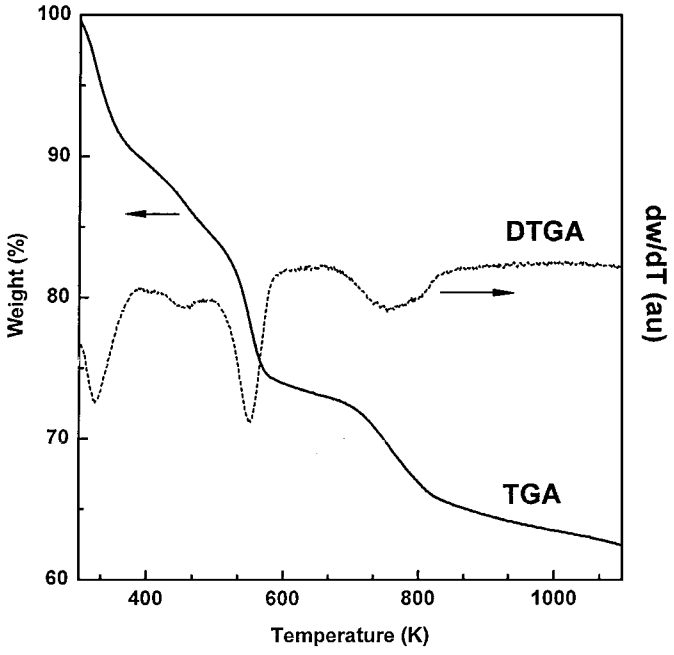


**FIG. 1.** Thermogravimetric curve (continuous line) and its derivative curve (dashed line) for the representative CZA-2 sample.

The X-ray diffraction (XRD) patterns of CZA precursors are shown in Fig. 2. For the sake of comparison, the powder diffraction profiles (bar diagrams) of some reference $(Cu, Zn)_2(OH)_3Cl$, $[NH_4Cu(NH_3)_2Cl_3]_{0.33}$, and $Cu_3Zn_3Al_2(OH)_{16}CO_3 \cdot 4H_2O$ compounds are also included in this figure. The presence of the ternary $Cu_xZn_{6-x}Al_2(OH)_{16}CO_3 \cdot 4H_2O$ hydrotalcite-like layered hydroxide is clearly observed in all the samples. The position of all diffraction peaks of this structure becomes slightly shifted depending on the Cu/Zn/Al ratio (14). This is illustrated by the compositions $x = 0$ with $d_{003}$ at 0.7600 nm (ICDD-PDF no. 38-486), $x = 2$ with $d_{003}$ at 0.7540 nm (ICDD-PDF no. 38-487), and $x = 3$ with $d_{003}$ at 0.7485 nm (ICDD-PDF no. 37-629). Since all these structures are isostructural with the hydrotalcite, the structure of these compounds can be described as an alternation between the cationic positions in the brucite sheet with $Cu^{2+}$ and $Zn^{2+}$ ions. The lattice parameter does not change to a significant value owing to the close dimensions of both cations. As reported (14), the best packing is obtained for a $Cu/(Cu + Zn)$ atom ratio close to 0.5. In fact, the hydrotalcite is the major phase in the precursor of CZA-3 sample in which the $Cu/(Cu + Zn)$ atom ratio is 0.40. Besides the major hydrotalcite structures, amminochloride $[NH_4Cu(NH_3)_2Cl_3]_{0.33}$ (ICDD-PDF no. 70-78), hydroxychloride $(Cu,Zn)_2Cl(OH)_3$ (ICDD-PDF no. 25-325 paratacamite, zincian), and $Cu_2Cl(OH)_3$ (ICDD-PDF no. 78-372 atacamite) are observed. All these compounds are formed as a consequence of the use of metal chloride precursors and urea as a precipitating agent. This is in contrast to the phases obtained in our previous study (2) by precipitating the nitrates of the corresponding cations with $Na_2CO_3$, in which a mixture of crystalline malachite, hydrozincite, and aurichalcite phases were dominant. The results clearly show that the synthesis route of the CZA precursors has a strong influence on the nature of phases developed.

The XRD patterns of CZA-1, CZA-2, and CZA-3 catalysts are shown in Fig. 3. For the sake of comparison, the ICDD powder diffraction profiles (bar diagrams) of reference CuO, ZnO, and $CuAl_2O_4$ compounds are also included in this figure. It is evident that diffraction lines of both CuO and ZnO phases are present in all calcined samples. In addition, samples CZA-2 and CZA-3 show not only the decrease of the intensity of ZnO relative to CuO phase but also the simultaneous appearance of broad components ($2\theta \sim 36.9^\circ$) of the $CuAl_2O_4$ phase. The crystal sizes ($d$) of CuO and ZnO phases for the three calcined CZA samples were calculated by using the Scherrer equation. The respective values are compiled in Table 1. The calculated $d$ values

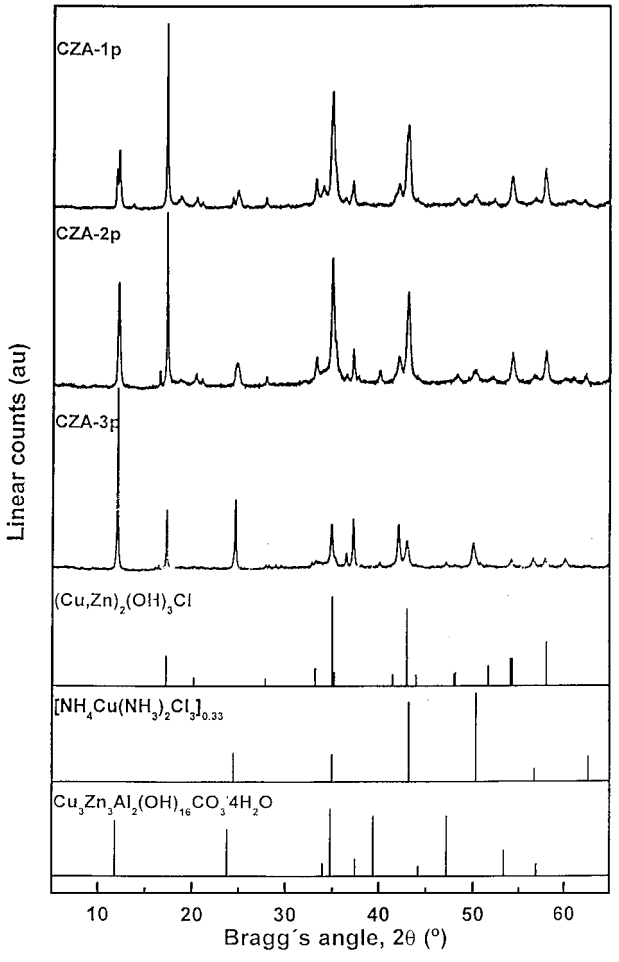


**FIG. 2.** Powder X-ray diffraction patterns of catalyst precursors. For the sake of phase identification, some chlorine-containing reference compounds (bar pattern) are included.

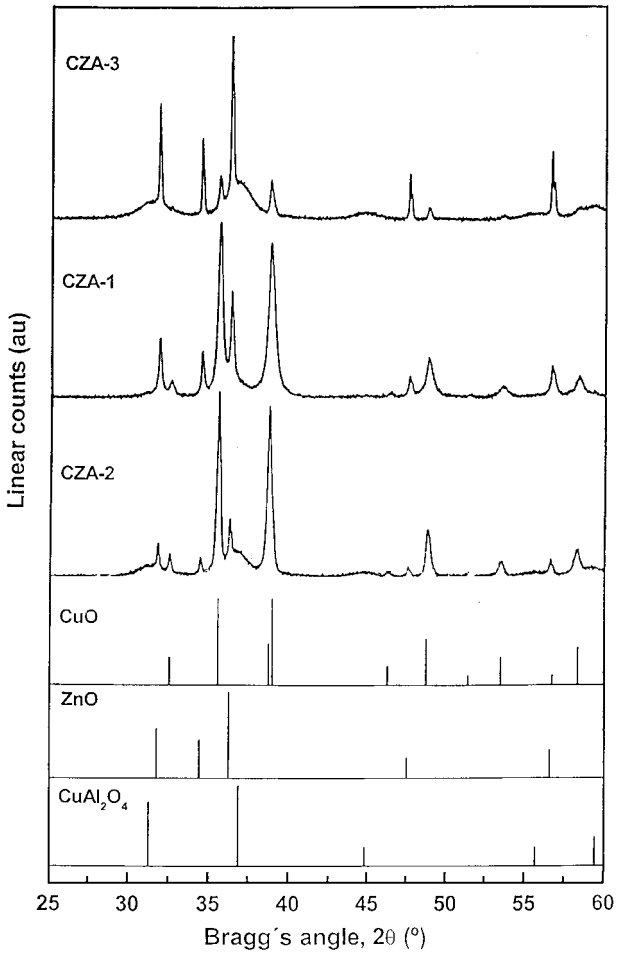


**FIG. 3.** Powder X-ray diffraction patterns of calcined catalysts CZA-1, CZA-2, and CZA-3. For the sake of phase identification, the ICDD-PDFs of the reference phases CuO (72-629), ZnO (36-1451), and $CuAl_2O_4$ (33-448) are also included.

of CuO are similar for the three samples (26–34 nm); however *d* values of ZnO are somewhat different. For CZA-1 and CZA-2, $d_{ZnO}$ values are 34 and 46 nm respectively, but increase up to 81 nm for the CZA-3 sample. In addition, the crystal size of the new observed $CuAl_2O_4$ phase in samples CZA-2 and CZA-3 was much smaller and close to 6 and 5 nm, respectively.

The TPR profiles of the three catalysts and bulk CuO sample as a reference are shown in Fig. 4. The TPR profile of the catalyst CZA-1 shows a peak at 573 K with a shoulder at the rising side of it. However, the reduction profiles of CZA-2 and CZA-3 samples show two sets of TPR peaks: one in the temperature range 400–520 K, and another in the range 550–750 K. In the low-temperature region up to three well-defined TPR peaks can be distinguished, and their intensity sharply increases with the Al content of the catalysts. Since for the CZA-2 and CZA-3 samples broad features at approximately $2\theta \sim 36.9^\circ$ suggest the appearance of crystalline $CuAl_2O_4$ structures, the set of TPR peaks located at low temperatures can reasonably be assigned to the reduction of copper in $CuAl_2O_4$-like species. In the high-temperature region, an asymmetrical TPR pattern, similar to that observed in sample CZA-1 (Fig. 4), although somewhat broadened with its maximum shifted to 653 K, is observed in sample CZA-2. For CZA-3 sample, this high-temperature TPR peak appears more broadened and asymetrical and shifts toward higher temperatures (maximum at 720 K). Calibration of TCD signal with a CuO standard (Merck, reagent grade) revealed that $H_2$ consumption corresponds in the three cases to the quantitative reduction of $Cu^{2+}$ to $Cu^o$.

The presence of a major $CuAl_2O_4$ phase in sample CZA-3, whose Al content and BET area are very high, favors copper dispersion and hence the reduction of $Cu^{2+}$ ions. In

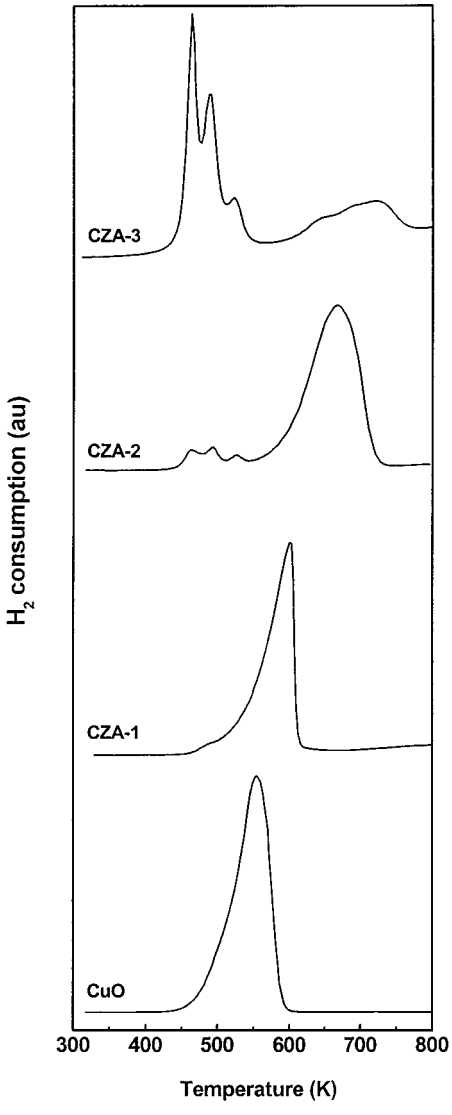


**FIG. 4.** Temperature-programmed reduction profiles for the calcined catalysts CZA-1, CZA-2, and CZA-3. Bulk CuO reference was also included for comparison.

our previous work (15), we already observed that highly dispersed copper in CZA catalysts would exhibit Cu–Al interaction in the calcined samples. The principal role of aluminum oxide would be to enhance the dispersion of oxidic copper species on its surface, both by the formation of a $CuAl_2O_4$ phase and by the stabilization of isolated $Cu^{2+}$ ions in the alumina matrix.

*Catalytic Activity*

The catalytic activities of the CZA catalysts, including a commercial BASF K3110 reference, in the POM at $O_2/CH_3OH$ feed ratios of 0.3 and 0.4 are shown in Figs. 5a and 5b, respectively. Similarly, activities of these catalysts in the OMR are displayed in Fig. 5c. For all the catalysts tested the main products of POM and OMR reactions were $H_2$, $H_2O$, CO, and $CO_2$. At low $O_2/CH_3OH$ ratio and low level of $CH_3OH$ conversion, significant amounts of formaldehyde together with very small amounts of dimethyl ether were also observed.

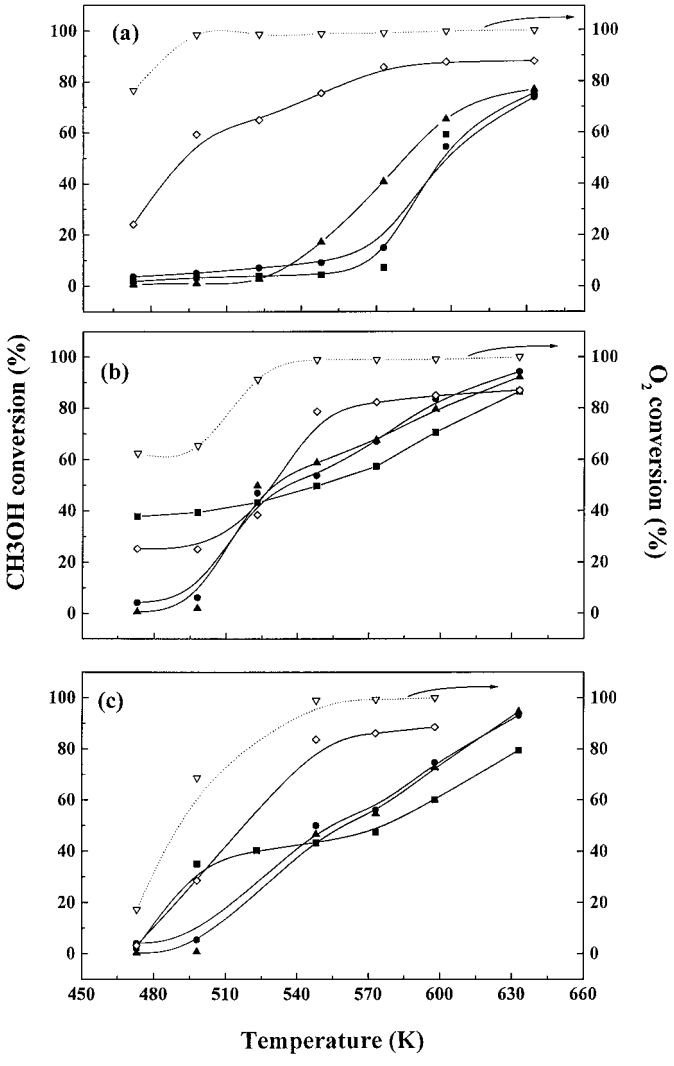


**FIG. 5.** Methanol conversion over CZA catalysts, (■), CZA1; (●), CZA2; (▲), CZA3, for POM reaction using feed ratios, (a) $O_2/CH_3OH = 0.3$ and (b) $O_2/CH_3OH = 0.4$, and OMR reaction (c) $O_2/CH_3OH/H_2O = 0.3/1/1.1$. $O_2$ (▽) and $CH_3OH$ (◇) conversions over a commercial catalyst are also included.

The CZA catalysts are very active for the POM reaction (Figs. 5a and 5b), showing a $CH_3OH$ conversion strongly influenced by reaction temperature. All the CZA samples show similar conversion patterns with a drastic increase in methanol and oxygen conversion in a narrow temperature range. This temperature interval depends on the catalyst composition and the $O_2/CH_3OH$ molar ratio used. For CZA samples, a decrease of approximately 40 K in this temperature interval was observed when the $O_2/CH_3OH$ molar ratio increases from 0.3 to 0.4. Working with $O_2/CH_3OH$ molar ratio of 0.3, the commercial catalyst is more active than all CZA samples in the whole range of temperatures investigated. However, $CH_3OH$ conversion over the commercial catalyst was limited at high temperatures (573–633 K); this is likely due to catalyst deactivation as a result of sintering of copper at high temperatures. Results in Figs. 5a and 5b show the increase of $CH_3OH$ conversion when increasing the $O_2/CH_3OH$ ratio from 0.3 to 0.4. This effect is less pronounced over the commercial catalyst, in which a decrease in $CH_3OH$ conversion is observed in the middle range of temperatures with increasing $O_2$ concentration in the feed. The activity decline may be linked to the oxidation of the copper surface (2). As already shown for the $O_2/CH_3OH$ molar ratio of 0.3, apparent deactivation (or kinetic effect) at temperatures higher than 573 K takes place in the commercial sample. Otherwise for the CZA samples there is no limitation in methanol conversion with temperature. Taking into account the large variation of the Cu, Zn, and Al content of the three CZA catalysts tested, there is not a clear relationship between catalyst composition and catalytic behavior in the POM reaction over these catalysts (Figs. 5a and 5b).

For the OMR reaction (Fig. 5c), all the CZA samples tested show values of $CH_3OH$ conversion higher than those attained under the conditions imposed by the POM reaction (Fig. 5a). A positive effect of steam and oxygen in the partial oxidation of methanol was already reported by Huang and Chren (10). The commercial catalyst still displays better $CH_3OH$ conversion than the CZA samples over the region of low reaction temperatures (<573 K). Notwithstanding, the commercial catalyst becomes deactivated at temperatures above 615 K, but deactivation is not observed in the CZA catalysts. Within the CZA series, CZA-3 and CZA-2 samples exhibit similar activities for all the temperatures tested, and are higher than that of the CZA-1 counterpart, although the latter catalyst is more active over the low-temperature interval (<543 K).

In order to get some insights into the mechanism of partial oxidation and oxidative reforming reactions of methanol over CZA catalysts, Table 2 illustrates the effect of temperature, $O_2/CH_3OH$ feed ratios, and $H_2O$

**TABLE 2**

**$CH_3OH$ Conversion, $O_2$ Conversion, and Product Distribution as Function of Temperature and $O_2/CH_3OH/H_2O$ Ratio over the Representative CZA-3 Catalyst**

| $O_2/CH_3OH/H_2O$ | 0.3/1/0 | | | 0.4/1/0 | | | 0.3/1/1.1 | | |
|---|---|---|---|---|---|---|---|---|---|
| $T$(K) | 498 | 568 | 598 | 498 | 568 | 598 | 498 | 568 | 598 |
| $CH_3OH$ conversion (%) | 1.1 | 17.1 | 65.1 | 1.9 | 58.8 | 79.5 | 0.8 | 46.6 | 72.6 |
| $O_2$ conversion (%) | 16.7 | 86.1 | 99.2 | 14.7 | 99.3 | 99.5 | 15.0 | 100 | 100 |
| Product selectivity | | | | | | | | | |
| $H_2$ | 23.8 | 8.2 | 65.5 | 28.6 | 56.5 | 64.1 | 22.7 | 62.8 | 66.9 |
| $H_2O$ | 45.3 | 58.1 | 0.03 | 38.7 | 9.2 | 1.2 | 58.4 | 2.1 | 0.0 |
| CO | — | 1.7 | 4.5 | — | 1.2 | 2.4 | — | 0.3 | 0.7 |
| $CO_2$ | 13.3 | 30.3 | 29.6 | 22.7 | 33.0 | 32.3 | 16.8 | 34.7 | 32.4 |
| Formaldehyde | 17.6 | 1.6 | 0.2 | 10.0 | — | — | 2.1 | — | — |
| Dimethyl ether | — | — | 0.1 | 0.0 | 0.05 | 0.05 | 0.0 | — | — |

incorporation on the $CH_3OH$ conversion and product distribution over the representative CZA-3 catalyst. The exit partial pressures of each product molecule and methanol reactant, obtained in POM reaction over the representative CZA-3 catalyst, as a function of temperature are plotted in Figs. 6 ($O_2/CH_3OH = 0.3$) and 7 ($O_2/CH_3OH = 0.4$). These results indicate clearly that both conversion and concentration of the products in the exit stream become strongly dependent on the $O_2$ concentration in the gas phase. At low-methanol conversion, when $O_2$ is not completely consumed,

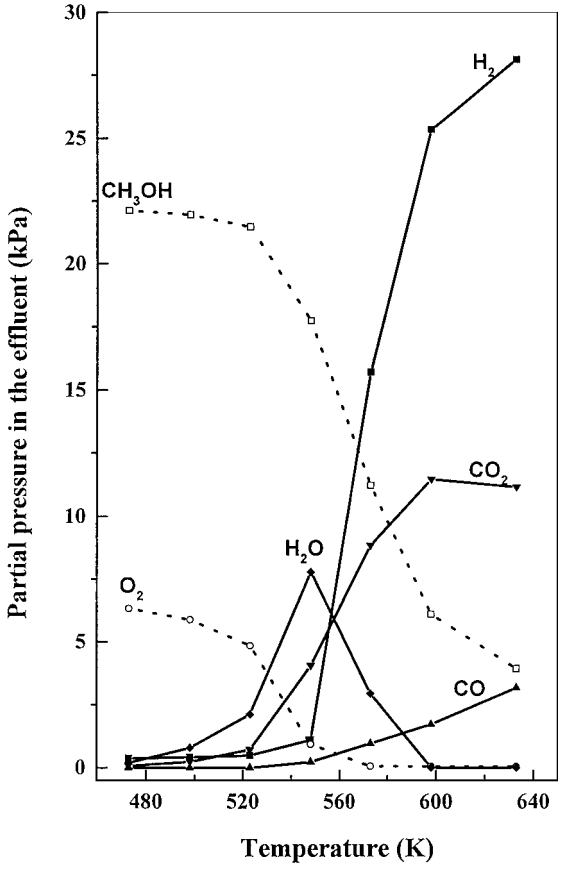


**FIG. 6.** Outlet partial pressure of the products (■), $H_2$; (◆), $H_2O$; (▲), CO; and (▼), $CO_2$ and reactants (□), $CH_3OH$ and (○), $O_2$ over the representative CZA-3 catalyst as a function of temperature during the POM reaction ($O_2/CH_3OH = 0.3$ molar ratio).

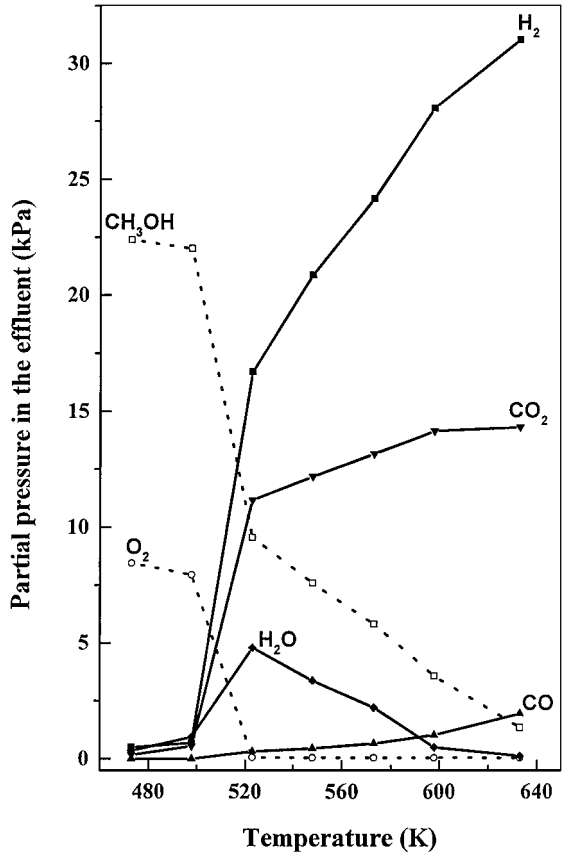


**FIG. 7.** Outlet partial pressure of the products (■), $H_2$; (◆), $H_2O$; (▲), CO; and (▼), $CO_2$ and reactants (□), $CH_3OH$ and (○), $O_2$ over the representative CZA-3 catalyst as a function of temperature during the POM reaction ($O_2/CH_3OH = 0.4$ molar ratio).

combustion and decomposition of methanol are the dominant reactions. When oxygen is near or completely consumed, the methanol conversion goes beyond the expected stoichiometric POM values (60 and 80% for $O_2/CH_3OH$ ratios of 0.3 and 0.4, respectively). The simultaneous increase in $H_2$ selectivity at the expense of water, with a less marked increase of CO selectivity, points to the contribution of steam reforming of methanol by the water byproduct.

The removal of oxygenate species along the methanol steam reforming process suggests that $CH_3OH$ reforming occurs, at least by reforming of these intermediate oxygenates. A similar reaction scheme of oxidation → reforming was previously reported by Cubeiro and Fierro (3) for the partial oxidation of methanol over a Pd/Zn catalyst. In the case of the steam reforming of methanol (Fig. 8), the concentration of the products in the efluent indicate that the reforming mechanism operates in the whole methanol conversion range, excluding the low conversion value, where the production of formaldehyde points to the contribution of partial methanol combustion (Table 2). A similar reaction mechanism and catalyst performance were found by Reitz *et al*. (16).

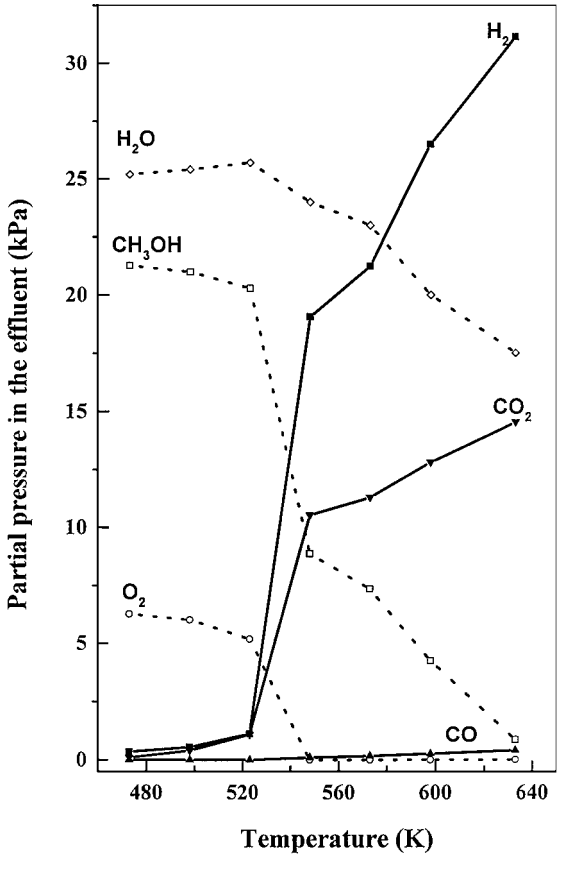


**FIG. 8.** Outlet partial pressure of the products (■), $H_2$; (▲), CO; and (▼), $CO_2$ and reactants (□), $CH_3OH$; (◇), $H_2O$; and (○), $O_2$ over the representative CZA-3 catalyst as a function of temperature during the oxyreforming of methanol ($O_2/CH_3OH/H_2O = 0.3/1/1.1$ molar ratio).

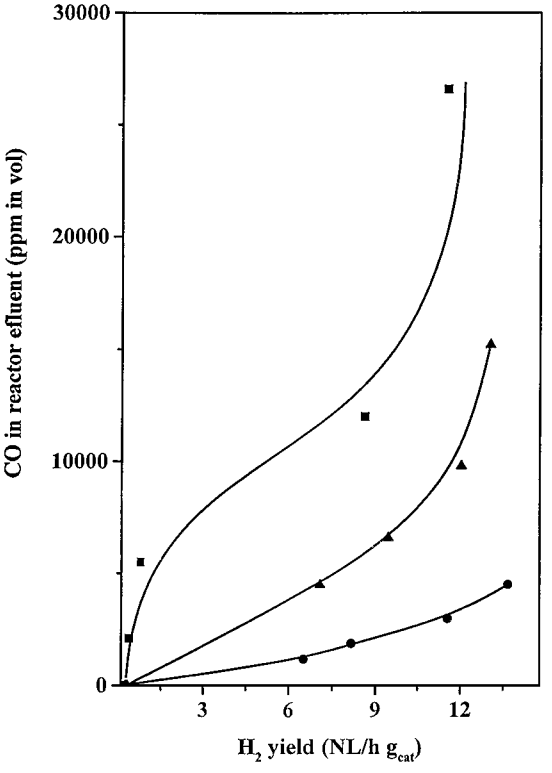


**FIG. 9.** CO concentration in the gas outlet as a function of hydrogen yield over the representative CZA-3 sample during the partial oxidation of methanol, (■), $O_2/CH_3OH = 0.3$ and (▲), $O_2/CH_3OH = 0.4$, and the oxyreforming of methanol, (●), $O_2/CH_3OH/H_2O = 0.3/1/1.1$.

As stated above, CZA catalysts are excellent candidates to be employed in both POM and ORM reactions. However, if the exit stream is intended to be used in fuel-cell applications, high hydrogen productions and low selectivities to CO are parameters of prime importance. For both POM and ORM reactions, all the CZA catalysts reach high $CH_3OH$ conversions with high selectivity toward $H_2$. However, the reaction conditions have strong influence on the CO selectivities obtained (Fig. 9). The CO selectivities increase in the order POM ($O_2/CH_3OH = 0.3$) > POM ($O_2/CH_3OH = 0.4$) > ORM. For the POM reaction, the decrease of both CO and $H_2$ selectivities and the simultaneous increase in $CO_2$ and $H_2O$ selectivity with increasing oxygen concentration in the feed suggest that CO and $H_2$ oxidations take place. The less marked effect on $H_2$ points to a faster oxidation of cabon monoxide. Addition of water to the feed stream strongly reduces the levels of CO achieved in POM reaction. Despite the complexity of the mechanism of oxidative reforming of methanol, it is likely that the water gas-shift reaction may contribute to the reduction of CO selectivities at the expense of water.

The nature of copper species present on the surface of calcined and used catalysts was revealed by XPS. The Cu 2*p* core-level spectra of the representative catalyst CZA-2, calcined and used in POM and ORM reactions, are displayed

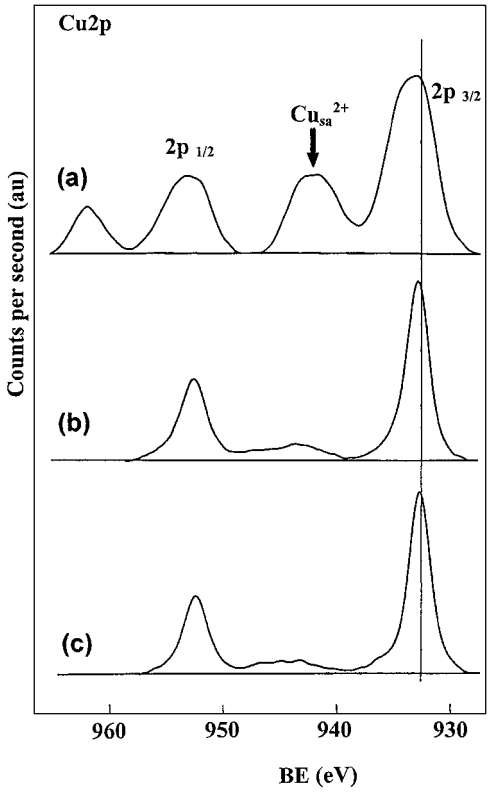


**FIG. 10.** Cu 2*p* core-level spectra of the representative CZA-2 catalyst, calcined (a), and used in the partial oxidation (POM) (b), and in the oxidative methanol reforming (OMR) (c) reactions.

in Fig. 10. The calcined catalyst shows an asymetric peak that can be deconvoluted in two components: at 933.4 eV assigned to CuO (17–20), and at about 935 eV related to $Cu^{2+}$ ions interacting with the hydroxyl groups of ZnO or in a $CuAl_2O_4$ spinel-type compound (15, 21). A $Cu^{2+}$ satellite peak is also observed at approximately 943 eV, which is the fingerprint of $Cu^{2+}$ ions (15, 22). Upon on-stream operation, the $Cu^{2+}$ satellite disappears and the principal Cu $2p_{3/2}$ peak shifts toward lower binding energy near 932.7 eV, which may be assigned to $Cu^o$ or $Cu^+$ (22). Since the binding energy of these reduced species is almost the same, to differentiate which of these species are present in the catalysts used, the modified Auger ($\alpha_A$) parameter was calculated (22). The $\alpha_A$ values of 1849.1 eV for the catalyst used in POM and 1849.3 eV for the OMR reaction are conclusive that $Cu^+$ species are present on the catalyst surface during stream operation (22). This finding is also consistent with the XRD patterns of the catalysts used in both reactions, which indicate the appearance of large $Cu_2O$ crystals on the catalyst surface.

In short, CuZnAl catalysts prepared from hydrotalcite-like precursors display excellent performance for hydrogen production via oxidative methanol reforming reactions. Particularly, the CZA-2 catalyst containing a 18.7% Al shows 100% selectively to $H_2$ at temperatures above 600 K; moreover CO, formaldehyde, and methylformate were under the detection limit on the whole temperature interval when working under the oxidative reforming conditions. Although the reaction scheme is very complex, the observation of oxygenate species at lower temperatures when the reaction is conducted under the POM conditions and their removal upon adding steam or increasing temperature suggest that $CH_3OH$ reforming occurs, at least in part, by reforming of intermediate oxygenates. Finally, measurement of the modified Auger parameter of copper in the catalysts used in both POM and OMR reactions indicates that $Cu^+$ species are present on the catalyst surface during on-stream operation.

## CONCLUSIONS

(i) A new method based on the homogeneous precipitation of chloride salts in the presence of urea has been applied for the preparation of CZA catalysts. The hydrotalcite and oxychloride precursors underwent thermal decomposition in air followed by activation in a reducing atmosphere.

(ii) The CZA catalysts so obtained were tested in both POM and OMR reactions, exhibiting high activity for $CH_3OH$ conversion and very high selectivity for $H_2$ production. The partial pressures of the products in the exit stream in the POM reaction as a function of temperature indicate clearly that composition become strongly dependent on the $O_2$ concentration in the gas phase. At low temperatures, where $O_2$ is not completely consumed, combustion and decomposition of methanol are the dominant reactions. When oxygen is near or completely consumed, the methanol conversion goes beyond the expected stoichiometric POM values (60 and 80% for $O_2/CH_3OH$ molar ratios of 0.3 and 0.4, respectively). The simultaneous increase in $H_2$ selectivity at the expense of water, with a less marked increase of CO selectivity, points to the contribution of steam reforming of methanol. For the three CZA catalysts studied, chemical composition does not influence the catalytic performance to a significant extent.

(iii) The chemical state of copper in the active catalysts was revealed by XRD and XPS-Auger spectroscopic techniques. Measurement of the modified Auger parameter of copper gave values of $Cu_{LMM}$ at 1849.1 eV for the catalyst used in POM ($O_2/CH_3OH = 0.3$) and at 1849.3 eV for the OMR ($O_2/CH_3OH/H_2O = 0.3:1:1.1$), which indicates that $Cu_2O$ species are present on the active catalyst surface. These $Cu_2O$ structures appear to be sufficiently large, also revealed from the XRD patterns of the catalysts used in both reactions.

## ACKNOWLEDGMENTS

Financial support of this work from CICYT, Spain under Grant QUI1998-0877, and from UE under Contract JOE3-CT97-0049 is acknowledged. Two of us (U.C. and M.N.) also thank the Italian MURST for financial support.

## REFERENCES


1. Kumar, R., Ahmed, S., and Krumpelt, M., *in* "1996 Fuel Cell Seminar Program and Abstracts," p. 750 (1996).
2. Alejo, L., Lago, R., Peña, M. A., and Fierro, J. L. G., *Appl. Catal.* **162**, 281 (1997).
3. Cubeiro, M. L., and Fierro, J. L. G., *J. Catal.* **179**, 150 (1998).
4. Takezawa, N., and Iwasa, N., *Catal. Today* **36**, 45 (1997).
5. Cubeiro, M. L., and Fierro, J. L. G., *Appl. Catal.* **168**, 307 (1998).
6. Jiang, C. J., Trimm, D. A., Wainwright, M. S., and Cant, N. W., *Appl. Catal.* **93**, 245 (1993).
7. Jiang, C. J., Trimm, D. A., Wainwright, M. S., and Cant, N. W., *Appl. Catal.* **97**, 145 (1993).
8. Peppley, B. A., Amphlett, J. C., Kearns, L. M., and Mann, R. F., *Appl. Catal.* **179**, 21 (1999).
9. Huang, T. J., and Wang, S. W., *Appl. Catal.* **24**, 287 (1983).
10. Huang, T. J., and Chren, S. L., *Appl. Catal.* **40**, 43 (1988).
11. Newson, E., Truong, T., and Hottinger, P., *Stud. Surf. Sci. Catal.* **130**, 695 (2000).
12. Cavani, F., Trifiro, F., and Vaccari, A., *Catal. Today* **11**, 173 (1991).
13. Costantino, U., Marmottini, F.; Nocchetti, M., and Vivani, R., *Eur. J. Inorg. Chem*. 1439 (1998).
14. Busetto, C., Del Piero, G., Manara, G., Trifiró, F., Vaccari, A., *J. Catal.* **85**, 260 (1984).
15. Figueiredo, R. T., Martinez-Arias, A., Lopez Granados, M., and Fierro, J. L. G., *J. Catal.* **178**, 146 (1998).
16. Reitz, T. L., Ahmed, S., Krumpelt, M., Kumar, R., and Kung H. H., *Stud. Surf. Sci. Catal.* **130A**, 3645 (2000).
17. Herman, R. G., Klier, K., Simmons, G. W., Finn, P. B., Bulko, J. B., and Kobylinski, T. P., *J. Catal.* **56**, 407 (1979).
18. Okamoto, Y., Fujino, K., Imanaka, T., and Teranishi, S., *J. Phys. Chem*. **87**, 3740 (1983).
19. Garbassi, F., and Petrini, G., *J. Catal.* **90**, 113 (1984).
20. Porta, P., Campa, M. C., Fierro, G., Lo Jacono, M., Minelli, G., Moretti, G., and Stoppa, L., *J. Mater. Chem*. **3**, 505 (1993).
21. Sepulveda, A., Marquez, C., Rodriguez, I., Guerrero, A., Fierro, J. L. G., *Surf. Interface Anal.* **20**, 1067 (1993).
22. See, e.g., Fierro, J. L. G., *Catal. Rev.-Sci. Eng.* **36**, 255 (1993), and references therein.